Journal of Computational and Applied Mathematics 429 (2023) 115211

Contents lists available at ScienceDirect

Journal of Computational and Applied Mathematics

journal homepage: www.elsevier.com/locate/cam

Towards an open-source framework for Fluid–Structure Interaction using SU2, MBDyn and preCICE

Alice Zanella, Luca Abergo *, Francesco Caccia, Myles Morelli, Alberto Guardone

Department of Aerospace Science and Technology, Politecnico di Milano, Building B12, Via La Masa 34, Milan, 20156, Italy

ARTICLE INFO

Article history:
Received 27 October 2022
Received in revised form 17 February 2023

ABSTRACT

Fluid–Structure Interaction (FSI) problems are a primary concern for the aerospace industry. Predicting the deformation of flexible structures due to aerodynamic forces is essential in different scenarios, e.g., for determining the performance of rotorcrafts and wind turbines. In this context, we present a new high-fidelity, open-source, modular, and user-friendly FSI simulation framework by coupling the well-established fluid solver SU2 with the multi-body structural solver MBDyn. The SU2 suite solves steady and unsteady Euler and RANS equations using a finite volume method on unstructured grids. The aerodynamic loads on the surfaces are then passed to MBDyn. Through a multi-body analysis, rotations, displacements, and the structural response of rotorcraft systems are efficiently computed and exchanged back with the fluid solver. A partitioned approach is used between the two codes, each specific for a single physical domain. Both explicit and implicit coupling were considered. The coupling is obtained through the library preCICE, which treats the two specialized solvers as "black boxes" and provides data mapping between non-matching grids. Classical FSI test cases are presented and results are compared with data from literature to validate the framework.

1. Introduction

The interaction between fluid and structure is a primary concern for the aerospace industry. It poses a challenging problem both numerically and computationally. Fluid–Structure Interaction (FSI) has a natural application in many aeronautical problems, e.g., the design of largely-deformable wings, Vertical Take-Off and Landing aircrafts, rotorcrafts and gust response [1]. Concerning helicopters, many structural solvers come with an in-house, low-fidelity aerodynamic model, which can reproduce the inflow and consequently trim the rotor. The increasing available computational power makes possible to introduce high-fidelity solvers and capture more complex phenomena, such as the blade-vortex interaction and the vortical wake. For this purpose, two specialized and separate solvers are usually employed. A Computational Structural Dynamics (CSD) code is used to model the blade dynamics, and a Computational Fluid Dynamics (CFD) solver is used to capture the aerodynamics of the rotor. The way data is exchanged between different domains is named coupling.

The application of FSI in rotorcraft studies became dominant in the 1980s. In 1986 Tung et al. coupled full-potential aerodynamic methods with comprehensive codes in a loosely-coupled transonic simulation using CAMRAD and full-potential rotor solver. In the 1990s, Bauchau and Ahmad developed a tightly-coupled solver using CAMRAD/JA and OVERFLOW to simulate the four-bladed UH-60 A Blackhawk helicopter rotor. In the early 2000s, finite element multi-body

* Corresponding author.
E-mail address: luca.abergo@polimi.it (L. Abergo).

https://doi.org/10.1016/j.cam.2023.115211
0377-0427/

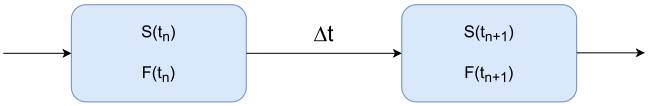

Fig. 1. Monolithic approach. S and F are the solid and the fluid operators. The advancing of the solution from time step t_n to t_{n+1} occurs simultaneously.

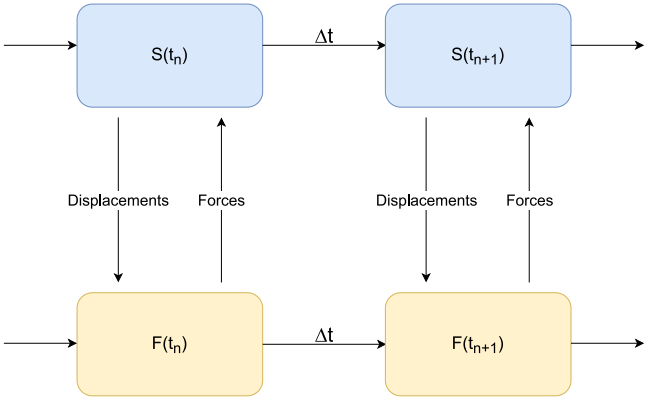

Fig. 2. Partitioned approach. S and F are the solid and the fluid operators. The fluid solver waits to receive the displacements from the structural solver, updates its solution and sends the forces to the structural solver. The time can advance and the loop repeats.

solvers were introduced to model rotor blade structural dynamics and control during rotorcraft operations [4]. These CSD codes use simplified aerodynamic models to reduce the computational cost.

Two coupling approaches are possible: *monolithic* and *partitioned*. In the *monolithic* approach, a single system of fluid and structural equations is solved at once (see Fig. 1). In this case, the interaction between fluid and structure at the mutual interface is explicitly inserted in the system and the conservation of quantities at the interface is straightforward [5–7]. With such an approach, only one solver would be responsible for both the fluid and the structural dynamics. In contrast, in the *partitioned* approach the fluid and the solid domains are treated separately and each is solved by a specialized code. They collide at the interface, where some conditions must be enforced. The data exchange and the coupling are performed by an additional module or external library. This approach could lack of unconditional stability: partitioned schemes are commonly energy-increasing. Therefore, the time-step must be smaller than in the monolithic approach [8]. The great advantage, though, is the freedom of coupling different solvers, managing the fluid and the solid domain discretization independently using two highly specialized codes (See Fig. 2).

The goal of this work is to create a completely open-source environment which can solve FSI problems with a very generalized structure. The framework is based on a partitioned approach with tight coupling, to guarantee both great flexibility and high accuracy. The open-source code SU2 [9] was chosen as fluid solver, while the open-source Multibody Dynamics solver MBDyn [10] handles the structural equations. The two codes are coupled using the library preCICE [11]. The integration is successfully verified on two test cases from literature, namely a vertical flap and a flexible cantilever in vortical flow.

The present paper is organized as follows. The framework and the software involved are shown in Section 2. Results of 2D test cases for verification and validation are shown in Section 3. In Section 4, the main findings and future perspectives are discussed.

2. Framework

This section introduces the individual solvers used for computing the aerodynamics and aeroelasticity of the problem. One adapter has been coded for each solver, and they communicate through the coupling library also introduced here. The framework can be deemed user-friendly since the FSI simulation is set with a unique text file.

2.1. Fluid domain and SU2

The SU2 suite deals with partial differential equations (PDEs) using a finite volume method on arbitrarily unstructured meshes. The PDEs are solved on a domain $\Omega \subset \mathbb{R}^3$ as long as they can be formulated as:

$$\frac{\partial \boldsymbol{U}}{\partial t} + \nabla \cdot \boldsymbol{F}^c(\boldsymbol{U}) - \nabla \cdot \boldsymbol{F}^v(\boldsymbol{U}) = \boldsymbol{Q} \quad \text{in } \Omega_f \times [0, t] \tag{1}$$

where $\boldsymbol{U}$ is the vector of conservative variables, $\boldsymbol{F}^c(\boldsymbol{U})$ are the convective fluxes, $\boldsymbol{F}^v(\boldsymbol{U})$ are the viscous fluxes and $\boldsymbol{Q}$ is a generic source term. From this general form a wide variety of PDEs can be derived, including the classical Euler, Navier–Stokes (NS) and Reynolds-Averaged Navier–Stokes (RANS) equations. For example, the NS equations are obtained considering:

$$\boldsymbol{U} = \begin{pmatrix} \rho \\ \rho \boldsymbol{v} \\ \rho e_0 \end{pmatrix}. \tag{2}$$

$$\boldsymbol{F}^c(\boldsymbol{U}) = \begin{pmatrix} \rho \boldsymbol{v} \\ \rho \boldsymbol{v} \otimes \boldsymbol{v} + \boldsymbol{I} p \\ \rho \boldsymbol{v} H + p \boldsymbol{v} \end{pmatrix}, \quad \boldsymbol{F}^v(\boldsymbol{U}) = \begin{pmatrix} \boldsymbol{0} \\ \boldsymbol{\tau} \\ \boldsymbol{\tau} \cdot \boldsymbol{v} + \kappa \nabla T \end{pmatrix} \tag{3}$$

where p denotes the static pressure, $\boldsymbol{I} \in \mathbb{R}^{3\times 3}$ is the identity matrix, H is the fluid enthalpy and $\boldsymbol{\tau}$ the viscous stress tensor. The heat conduction has been discretized with the Fourier law, with κ being the thermal conductivity and T the temperature.

For FSI, it is convenient to rewrite the fluid equations in an Arbitrary Lagrangian Eulerian (ALE) formulation. In this case, the vector of the convective fluxes $\boldsymbol{F}^c(\boldsymbol{U})$ must be rewritten as:

$$\boldsymbol{F}^c_{ALE}(\boldsymbol{U}) = \begin{pmatrix} \rho(\boldsymbol{v} - \dot{\boldsymbol{u}}_\Omega) \\ \rho \boldsymbol{v} \otimes (\boldsymbol{v} - \dot{\boldsymbol{u}}_\Omega) + \boldsymbol{I} p \\ \rho(\boldsymbol{v} - \dot{\boldsymbol{u}}_\Omega) e_0 + p \boldsymbol{v} \end{pmatrix} \tag{4}$$

with $\dot{\boldsymbol{u}}_\Omega$ being the velocity of the arbitrarily moving nodes of the grid.

The numerical methods used for solving the Unsteady Reynolds Averaged Navier Stokes (URANS) equations are hereinafter discussed. A second order Backward differentiation formula (BDF2) with dual time-stepping is used as time discretization [12]. Dual time-stepping is particularly appropriate for unsteady problems and can increase accuracy, provided that convergence is reached. A multi-grid technique has also been used to speed up convergence [13]. The Roe method with MUSCL reconstruction was used as second order accurate convective scheme. SU2 also provides a mesh deformation technique, called Radial Basis Function (RBF). RBF is able to apply large deformations preserving the quality of the grid, with a relative cheap computational cost [14,15].

2.2. Structural domain and MBDyn

MBDyn [16] is free and open-source general purpose Multibody Dynamics analysis software developed at the Department of Aerospace Science and Technology of Politecnico di Milano. The code offers a multibody dynamics approach to analyse complex, multidisciplinary dynamics problems. MBDyn can simulate linear and non-linear dynamics of rigid and flexible bodies (lumped elements, beams, or shells) subject to kinematic constraints, rotations, external forces, and control subsystems. MBDyn can integrate aerodynamic, electric, thermal, and hydraulic models with the structural domain. For a mid-fidelity approach, it offers inflow models, which are used to simulate fixed-wing and rotorcraft aerodynamics and enable fast analysis of various flight conditions. The calculation time is comparably short, as opposed to three-dimensional finite element formulations [17]. It makes multibody analysis a very efficient simulation tool for rotorcraft systems.

Nodes are the fundamental MBDyn entities: they instantiate kinematic degrees of freedom (DoF) and the corresponding equilibrium equations. Different types of nodes exist in MBDyn. In this work, dynamic nodes are used. Each node can have up to 6 DoF, i.e., the three coordinates defining its position and the three Euler-like angles defining its orientation (following the 1, 2, 3 convention), and also store all the information regarding the inertia. Elements are used to connect nodes, can access nodal properties and write contributions to the equations. In this context, three-node, second-order beam elements are used. Beams are particularly useful when dealing with slender bodies, as rotor blades [18] or wind turbines [19], in order to reduce the order of complexity to a 1D model. Deformable, slender beams are implemented in MBDyn using the Finite Volume approach explained by [20]. They are defined by a reference line and its nodes. Each point of the beam refers to a structural node. An arbitrary offset is allowed to guarantee more freedom in defining the reference line. At each evaluation point, a 6D constitutive law must be defined, relating the strains and the curvatures of the beam to the internal forces and moments at the evaluation points. Various constitutive laws are implemented, ranging from the isotropic beam section to the fully anisotropic one. In this work, a linear viscoelastic law is chosen.

In practice, MBDyn solves Newton–Euler equations of motion for rigid bodies connected by kinematics joints and deformable elements. Lagrange multipliers λ are used to impose constraints. Thus, a system of differential–algebraic equations is solved:

$$M(x)\dot{x} = q \tag{5}$$

$$\dot{q} + \frac{\partial \phi}{\partial x}\lambda = f(x, \dot{x}, t) \tag{6}$$

$$\phi(x, t) = 0 \tag{7}$$

where x are the kinematic variables, including rotations, q the momentum and momenta moments, and $\phi(x, t) = 0$ the imposed blade pitch and rotations, added as algebraic relations between the Cartesian coordinates of the bodies.

An A/L stable, multi-step integration scheme is used for time marching [21]. An incremental approach is used with a predictor–corrector scheme to compute the orientation between two consecutive time steps. The guess increment remains constant, while the corrector operator is formulated in terms of Cayley–Gibbs–Rodrigues parameters, which does not use trigonometric operations [22].

2.3. Coupling with preCICE

The coupling library preCICE is developed by the Technical University of Munich (TUM), the University of Stuttgart and the University of Erlangen. It offers the possibility to couple single-physics specialized software in a partitioned multi-physics simulation, treating them as "black-boxes". Indeed, no knowledge about the inner processes of the solvers is required by the library. One of the main advantages of preCICE is flexibility. It provides technical communication, data mapping between non-matching grids, and coupling iteration schemes.

Four variables control the interaction between solvers. The coupling step can run parallel or serial, in an either explicit or implicit manner. The choice is crucial, not only because of the different execution time of an iteration, but also because of the instabilities that could arise [23]. The explicit serial coupling is typically called *conventional serial staggered* and provides to the fluid solver F^n the solid solution at the current time step, s^n. The new flow variables, f^{n+1} are transmitted to the structural solver S^n to compute the new structural solution s^{n+1}:

$$f^{n+1} = F^n(s^n) \tag{8}$$

$$s^{n+1} = S^n(f^{n+1}) \tag{9}$$

The explicit scheme can be accelerated with a parallel implementation, where the two solvers F^N and S^N are executed at the same time using the solutions f^n and s^n. This, however, usually introduces a loss of accuracy and stability. Therefore, this method is not considered in this work [24]. Instability issues can be overcome with implicit schemes. In preCICE, implicit schemes are based on fixed-point iterations. Within the same time instance, the coupling conditions at the FSI interface are enforced and the following set of equations is solved iteratively:

$$f_{k+1}^{n+1} = F^n(s_k^{n+1}) \tag{10}$$

$$s_{k+1}^{n+1} = S^n(f_k^{n+1}) \tag{11}$$

where k labels the sub-iterations of the fixed-point method. The sub-iterations stop when the following convergence criteria are satisfied:

$$\left. \frac{\hat{f}_{k+1}^{n+1} - \hat{f}_k^{n+1}}{\hat{f}_k^{n+1}} \right|_\Gamma < \mathrm{tol}_f \tag{12}$$

$$\left. \frac{\hat{s}_{k+1}^{n+1} - \hat{s}_k^{n+1}}{\hat{s}_k^{n+1}} \right|_\Gamma < \mathrm{tol}_s \tag{13}$$

where $\hat{f}_\square^\square|_\Gamma$ and $\hat{s}_\square^\square|_\Gamma$ are, respectively, the fluid forces and the structural displacements evaluated on the interface Γ between the two domains, while tol_f and tol_s are the chosen threshold values.

The need of data mapping is typically related to a fluid mesh finer than the solid one. Thus, at the interface there are more fluid nodes than structural ones. Moreover, in our framework, the information coming from and fed to MBDyn by the adapter belongs to a 1D space, while SU2 uses grids made of 2D or 3D elements. The mapper should not disrupt the mass and energy balances. Therefore, preCICE offers different methods to correctly map data between different domains, either in a consistent or conservative form. In consistent mapping, the value assigned to a structural node is the same as the value assigned to the corresponding fluid nodes. Thus, consistent mapping is used for displacements and all fluid nodes assigned to that single solid node experience the same movement. The conservative form, on the other hand, ensures that the integral value is preserved. Forces require this property. Their value at a structural node must be equal to the integral on the associated fluid nodes.

Different mapping strategies are implemented. The main ones are *Nearest Neighbour*, *Nearest Projection*, and *Radial Basis Functions*. The Nearest Neighbour only requires vertex position information. The value at one node on the source mesh is assigned to the closest node of the target mesh, in Euclidean distance (Fig. 3). This results in first order accuracy. It is computationally cheap and works well when the two grids are almost coincident. The Nearest Projection requires an additional source of information, i.e., the connectivity of the source mesh. The target mesh points are projected on the mesh elements of the source mesh. Then, the method performs linear interpolation on them and assigns the interpolated values back on the target mesh. It is second order accurate. A 3D representation is given in Fig. 4. Finally, a Radial Basis Function (RBF) does not require any topological information and works well on most grids. Gaussian and thin plate splines are available as basis functions. The computational complexity of the data mapping can be reduced using a local support for the basis functions. This means that the spatial influence of nodes, from which data is mapped, is limited to a certain range, called *support radius*.

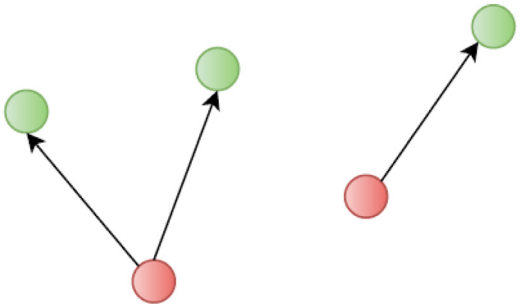

Fig. 3. Nearest neighbour method: shortest euclidean distance.

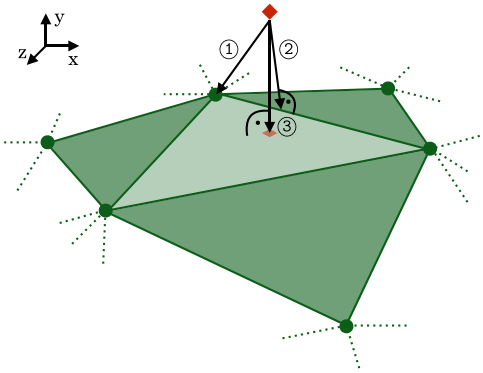

Fig. 4. Nearest projection method for a 3D case.
Source: Figure taken from [25].

3. Results

Two bi-dimensional test cases on simple flows are carried out to verify and validate the reliability of the coupling. The first one is a simple 2D vertical beam that interacts with a fluid experiencing large deformations. The aim is to verify the coupling of MBDyn and SU2 by comparing the results with other known couplings found on the preCICE repository.[1] The second test-case serves as validation. It is a well known FSI benchmark described in [26]. It consists of a square cylinder with a trailing flap crossed by a viscous, laminar flow. The computational aspect is more involved, since the flap oscillates along with complex vortex structures. After a grid sensitivity analysis, the results are compared with literature. Concerning the mapping of forces and displacements, for both the test cases Nearest Projection is used to map the displacements from the 1D structural grid to the fluid mesh, whereas the loads are mapped using RBF. In this way, only the connectivity of the beam nodes is shared with preCICE, which is computationally less expensive than sharing the connectivity of the fluid mesh.

3.1. Verification test case: Perpendicular flap

This first test case is a 2D simulation of a deformable flap which extends in a channel. The fluid flows horizontally through the channel, while the flap stands vertically. At the lower end the flap is clamped to the floor, while the upper part can move freely. Fig. 14 shows the geometry of the test case. All the fluid and structural properties, the SU2 setup and grid are taken from the preCICE tutorial repository. In this way, it is possible to compare the new MBDyn-preCICE-SU2 framework with other software. In particular, preCICE has been used to couple SU2 with two Finite Elements solvers, FEniCSx [27] and Calculix (See Fig. 5).[2]

The flow is assumed compressible and inviscid, and therefore governed by the Euler equations. The flow domain is discretized using an unstructured grid provided by preCICE website. The fluid and solid properties are listed in Table 1. The MBDyn model is composed of 10 s order beam elements. It was seen that by doubling the number of beam elements, the maximum tip displacement changes by less than 0.1%. The 10 beams are connected to 9 nodes, plus 2 at the extremities.

[1] preCICE test cases: https://github.com/precice/tutorials. Accessed Sept. 2022.
[2] Calculix Website: https://github.com/calculix. Accessed Sept. 2022.

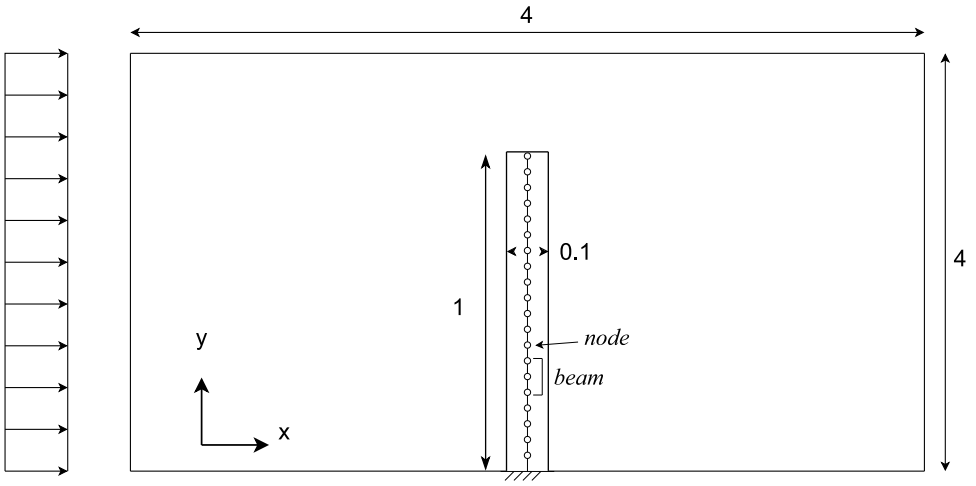

Fig. 5. Domain of the 2D flap test case. The structural discretization is also highlighted.

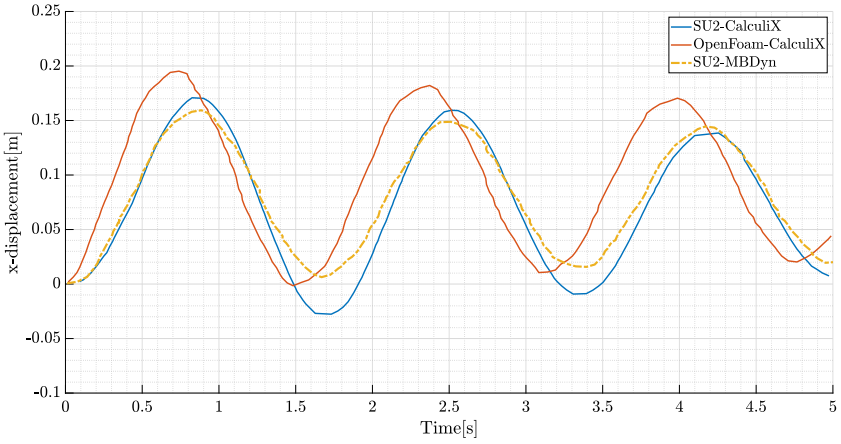

Fig. 6. Tip displacement: Result Comparison with Precice Website Data.

Table 1
Vertical flap test case: fluid and solid properties.

Quantity	Symbol	Value	Unit
Fluid Density	ρ	1	$\mathrm{kg\,m^{-3}}$
Kinematic Viscosity	ν	10^{-3}	$\mathrm{m^2\,s^{-1}}$
Mach	M	0.1	
Solid Density	ρ	3000	$\mathrm{kg\,m^{-3}}$
Elastic Modulus	E	$4 \cdot 10^6$	Pa
Poisson Coefficient	ν	0.3	
Damping Factor		0.0001	

Moreover, each second order beam intrinsically has an additional node in its centre. The discretization of the flap is highlighted in Fig. 14. The beam is clamped at one end and free at the other. In this case, the nodes have only two degrees of freedom, the orientation is not included in the kinematic variables.

The FSI simulation is started from the single-physics fluid solution, in order to let the flow field to fully develop and speed up convergence. Implicit and explicit coupling provide the same tip displacement history. A time step of 0.05 s is used. RBF is used for mapping displacements and forces. The expected behaviour is observed: the flap bends in the direction of the flow and then oscillates back and forth for three times. The maximum tip displacement is slightly lower with respect to the other FSI frameworks using SU2. The frequency, however, is well captured as can be seen in Fig. 6. The difference can be attributed to the extremely simple 1D, 2 DoF beam model used in this test case, while the other results reported use 2D structural elements.

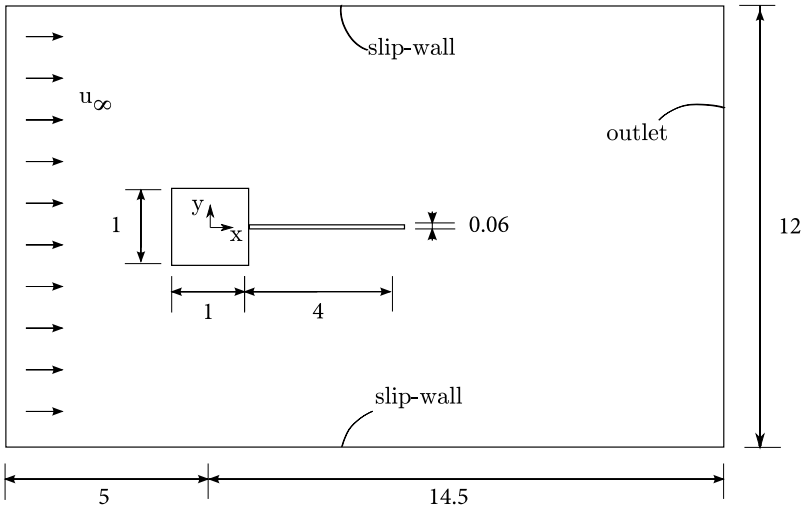

Fig. 7. Fluid domain for the bluff body with flexible cantilever. Distances are shown in cm.

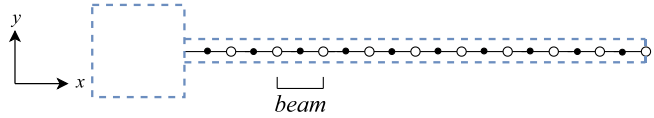

Fig. 8. Flexible cantilever structure. Evidence on beams and nodes.

Table 2
Bluff body with flexible cantilever: fluid and solid properties.

Quantity	Symbol	Value	Unit
Inlet Velocity	u_∞	0.513	$m\,s^{-1}$
Fluid Density	ρ_f	1.18	$kg\,m^{-3}$
Kinematic Viscosity	ν_f	1.54×10^{-5}	$m^2\,s^{-1}$
Temperature	T	0.0164	K
Reynolds Number	Re	332	
Mach Number	M	0.2	
Solid Density	ρ_s	100	$kg\,m^{-3}$
Elastic Modulus	E	0.25	MPa
Poisson Coefficient	ν_s	0.35	
Damping Factor		0.005	

3.2. Validation test case: Flexible cantilever in vortical flow

The problem consists of a fixed square bluff body, with a flexible flap attached to it. The body is immersed in a laminar, compressible flow. The test case was first proposed by [26]. It has been used as a benchmark FSI problem by many authors (see Table 3). The 2D physical domain is shown in Fig. 7. The square cylinder sheds vortices, which generate an area of low-pressure on its wake perceived by the flexible appendix. This alternated force generates vortex-induced vibrations on the structure, finally resulting in a structure driven vortex shedding. In the literature, the frequency of the flap oscillation and the maximum amplitude of the vertical displacement at the cantilever tip are extensively used for validation. The reported frequencies are in the range 3.0 Hz to 3.2 Hz, while the tip displacements lie between 0.95 cm and 1.31 cm.

Concerning the fluid domain, the square and the flap are non-slip walls, while the upper and the lower boundaries are slip walls. Due to the low Reynolds number, and the non-negligible Mach number, the compressible Navier–Stokes equations are solved. The physical properties of the flow are shown in Table 2 together with the solid properties of the cantilever beam. Its thickness as well as the material properties are chosen so that its first eigen-frequency is close to the frequency of the vortex shedding. The beam is clamped at the left end and free at the other. The beam section is uniform and the physical properties are constant throughout the beam length. A linear viscoelastic constitutive law is chosen, with a damping factor of 0.005. A representation of the MBDyn model of the flexible appendix is shown in Fig. 8.

Since the problem is strongly coupled, an implicit scheme is chosen. The simulation is started from a converged flow solution computed with a rigid flap, in order to speed up the transient.

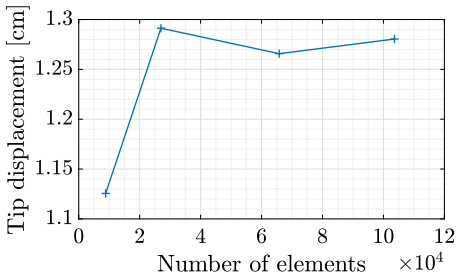

Fig. 9. Convergence of the maximum tip displacement by increasing the number of elements in the fluid domain.

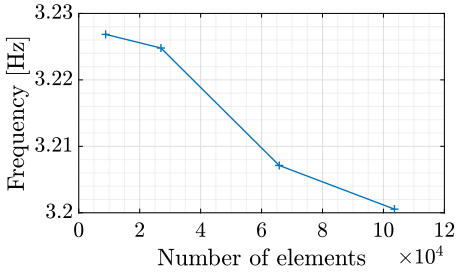

Fig. 10. Convergence of the vibration frequency of the beam by increasing the number of elements in the fluid domain.

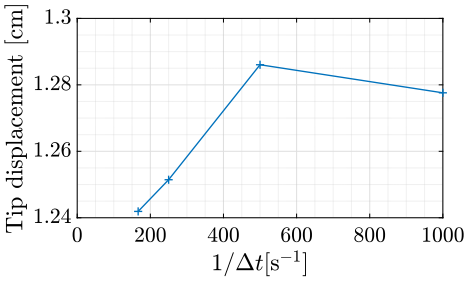

Fig. 11. Convergence of the maximum tip displacement by increasing the sampling frequency in the time domain.

The discretization of the structural domain was kept fixed, considering once more 10 s order beam elements defined using a total of 21 structural nodes. On the other hand, the solution showed strong dependence on the spatial discretization of the flow domain and on the temporal discretization. The results of space and time convergence are shown in Figs. 9 to 12. A too coarse spatial discretization affects the maximum tip displacement of the beam (Fig. 9), where the relative error between the two coarsest grids is about 12%. On the other hand, the relative error on the vibration frequency of the beam was always below 1% and decreased as the number of elements of the fluid domain increased. On the other hand, the time discretization affected both the maximum tip displacement of the beam and its vibration frequency in a similar manner. The relative error decreased below 1% with a sampling frequency of 500 Hz.

The evolution of the flow field is shown in Fig. 13. Initially, vortex shedding generates from the square as a result of the sharp edges. Then, this vortex trail causes the flap to start to oscillate, which results in another vortex trail detaching. This work presented a tip displacement of 1.28 cm and a frequency of oscillation of 3.20 Hz, with a Strouhal number of 0.062. The values agree well with other studies found in literature. A comparison is reported in Table 3.

4. Conclusion

In this paper, a new framework for fluid–structure interaction with partitioned approach was described. The structural solver MBDyn was linked with the fluid solver SU2 using the coupling library preCICE. Within this framework, implicit and explicit couplings can be used, and different mapping techniques are also available. The framework is modular, highly specialized, user-friendly and totally open-source. The need for an open-source solver arises from the fact that many existent couplings employ two closed-source solvers and do not allow any modification of the source code. Therefore, developers could not modify and improve the capabilities and extend the possible applications.

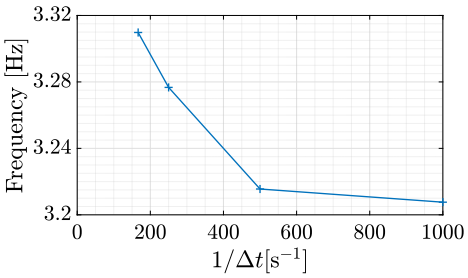

Fig. 12. Convergence of the vibration frequency of the beam by increasing the sampling frequency in the time domain.

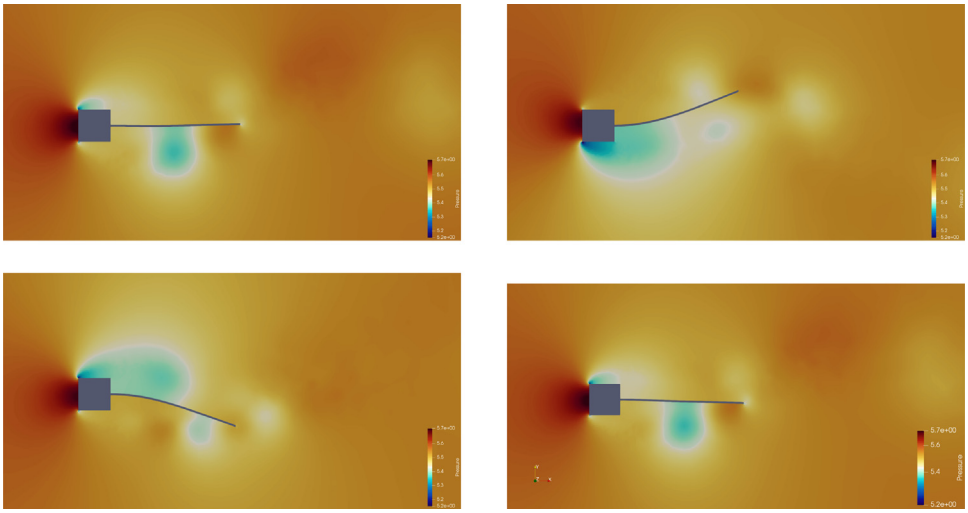

Fig. 13. Bluff body with flexible cantilever: pressure visualization of the flow field in different phases. Low-pressure regions are represented in cyan. Top left: $t \approx 0$. Top right: $t \approx \frac{1}{3}T$. Bottom left: $t \approx \frac{2}{3}T$. Bottom right: $t \approx T$.

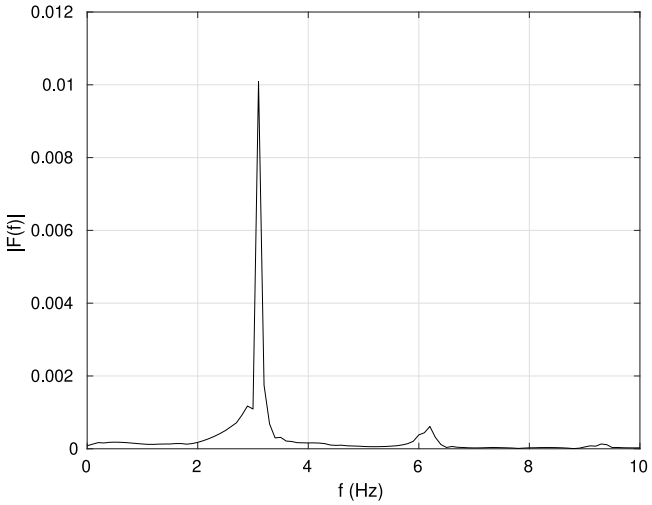

Fig. 14. Bluff body with flexible cantilever: FFT plot representing the oscillation frequency.

The verification of the proposed framework was made with two test cases. They proved the robustness of the mesh mapping and data exchange. The first one was a flexible vertical flap immersed in an inviscid flow. The second was a flexible flap behind a bluff body immersed in a viscous, laminar flow, which is a largely studied case in the context of fluid–structure interaction simulations. The results showed good agreement with literature.

```
<solver-interface dimensions="2">

   <!-- === Data ================================================ -->
   <data:vector name="Forces0" />
   <data:vector name="DisplacementDeltas0" />

   <!-- === Mesh ================================================ -->
  <mesh name="SU2_Mesh0">
     <use-data name="Forces0"/>
     <use-data name="DisplacementDeltas0"/>
   </mesh>

   <mesh name="MBDyn_Mesh0">
     <use-data name="DisplacementDeltas0" />
     <use-data name="Forces0" />
   </mesh>

   <!-- === Participants ======================================== -->
   <participant name="SU2_CFD">
     <use-mesh   name="MBDyn_Mesh0" from="MBDyn" geometric-filter="no-filter"/>
     <use-mesh   name="SU2_Mesh0"  provide="yes" />
     <write-data name="Forces0"              mesh="SU2_Mesh0" />
     <read-data  name="DisplacementDeltas0" mesh="SU2_Mesh0" />
     <mapping:nearest-neighbor direction="write" from="SU2_Mesh0"  to="MBDyn_Mesh0"
       constraint="conservative" />
   </participant>

   <participant name="MBDyn">
     <use-mesh   name="MBDyn_Mesh0" provide="yes"/>
     <write-data name="DisplacementDeltas0"   mesh="MBDyn_Mesh0" />
     <read-data  name="Forces0"               mesh="MBDyn_Mesh0" />
     <mapping:nearest-projection direction="read"  from="MBDyn_Mesh0" to="SU2_Mesh0"
       constraint="consistent" />
   </participant>

   <!-- === Communication ======================================= -->
   <m2n:sockets exchange-directory="./../" from="MBDyn" to="SU2_CFD"/>

   <!-- === Coupling scheme ===================================== -->
   <coupling-scheme:serial-implicit>
     <participants first="SU2_CFD" second="MBDyn" />
     <max-time value="20.0" />
     <time-window-size value="1e-3" />
     <exchange data="Forces0"   mesh="MBDyn_Mesh0"         from="SU2_CFD" to="MBDyn" />
     <exchange data="DisplacementDeltas0"    mesh="MBDyn_Mesh0"  from="MBDyn"  to="SU2_CFD" />
     <max-iterations value="100"/>

     <relative-convergence-measure limit="1e-4" data="DisplacementDeltas0" mesh="MBDyn_Mesh0" />
     <relative-convergence-measure limit="1e-4" data="Forces0" mesh="MBDyn_Mesh0"/>

```

Fig. A.15. Configuration File.

Table 3
Bluff body with flexible cantilever: summary of results.

	Average frequency [Hz]	Max tip displacement [cm]
Ramm and Wall [26]	3.08	1.31
Matthies and Steindorf [28]	2.99	1.33
Dettmer and Perić [29]	2.96–3.31	1.1–1.4
Wood et al. [30]	2.78–3.125	1.1–1.2
Kassiotis et al. [31]	3.17	1.0
C. et al. [32]	3.25	1.02
Froehle and Persson [33]	3.18	1.12
Present study	3.20	1.28

Since MBDyn is highly specialized on multi-body models undergoing rotations and SU2 is capable of producing high-fidelity flow simulations on rotorcraft [34], the natural extension of this work will be the 3D fluid–structure coupled simulation of helicopter rotors.

Code availability

The framework is composed by two solvers, SU2 and MBDyn, the coupling library preCICE and two adapters. The softwares can be found:

- MBDyn https://www.mbdyn.org/
- MBDyn adapter https://gitlab.com/stilita/mbdyn-esm-adapter/
- preCICE https://precice.org/

- SU2 ver 7.5 https://github.com/su2code/SU2
- SU2 ver 6 adapter https://github.com/precice/su2-adapter

Accessed: 2 February 2023.

Data availability

Data will be made available on request.

Appendix. FSI configuration file

In this appendix, it is explained how to set the general configuration file for the fluid–structure simulation. This XML-formatted file contains all the data required for the interface, instead the grids and the settings of each domain are in a dedicated folder. Taking ad reference Fig. A.15, the first line explicit the physical dimension of the problem. From line 3 to 6, it is indicated which fields are exchanged between the domains. Then, the config file requires the name of the grids and what are the input and the output of each domain. From line 18 to 34, the user must indicate the name of the solvers' executable and the mapping technique desired. The line 37 indicates the path between the folders containing the grid and config file of each solver. From line 39 to line 49, it is declared the type of coupling. In the figure, it is reported an implicit coupling which requires to explicit more options such as in which sequence the solvers are called, the maximum number of coupling iterations and the criteria of convergence.

References

[1] P. Sváček, J. Horáček, On mathematical modeling of fluid–structure interactions with nonlinear effects: Finite element approximations of gust response, J. Comput. Appl. Math. 273 (2015) 394–403, http://dx.doi.org/10.1016/j.cam.2014.05.006.
[2] C. Tung, F.X. Caradonna, W.R. Johnson, The prediction of transonic flows on an advancing rotor, J. Am. Helicopt. Soc. 31 (3) (1986) 4–9, http://dx.doi.org/10.4050/JAHS.31.3.4.
[3] O. Bauchau, J. Ahmad, Advanced CFD and CSD methods for multidisciplinary applications in rotorcraft problems, in: 6th Symposium on Multidisciplinary Analysis and Optimization, AIAA, NASA and ISSMO, 1996, pp. 1441–1451, http://dx.doi.org/10.2514/6.1996-4151.
[4] O. Bauchau, C. Bottasso, Y. Nikishkov, Modeling rotorcraft dynamics with finite element multibody procedures, Math. Comput. Modelling 33 (10) (2001) 1113–1137, http://dx.doi.org/10.1016/S0895-7177(00)00303-4.
[5] B. Hübner, E. Walhorn, D. Dinkler, A monolithic approach to fluid-structure interaction using space-time elements, Comput. Methods Appl. Mech. Engrg. 193 (2004) 2087–2104, http://dx.doi.org/10.1016/j.cma.2004.01.024.
[6] C. Michler, S. Hulshoff, E. van Brummelen, R. de Borst, A monolithic approach to fluid–structure interaction, Comput. & Fluids 33 (5) (2004) 839–848, http://dx.doi.org/10.1016/j.compfluid.2003.06.006, Applied Mathematics for Industrial Flow Problems.
[7] F.J. Blom, A monolithical fluid-structure interaction algorithm applied to the piston problem, Comput. Methods Appl. Mech. Engrg. 167 (3) (1998) 369–391, http://dx.doi.org/10.1016/S0045-7825(98)00151-0.
[8] S. Piperno, C. Farhat, B. Larrouturou, Partitioned procedures for the transient solution of coupled aroelastic problems part I: Model problem, theory and two-dimensional application, Comput. Methods Appl. Mech. Engrg. 124 (1) (1995) 79–112, http://dx.doi.org/10.1016/0045-7825(95)92707-9.
[9] T.D. Economon, F. Palacios, S.R. Copeland, T.W. Lukaczyk, J.J. Alonso, SU2: An open-source suite for multiphysics simulation and design, Aiaa J. 54 (3) (2015) 828–846, http://dx.doi.org/10.2514/1.J053813.
[10] P. Masarati, M. Morandini, P. Mantegazza, An Efficient Formulation for General-Purpose Multibody/Multiphysics Analysis, J. Comput. Nonlinear Dyn. 9 (4) (2014) http://dx.doi.org/10.1115/1.4025628.
[11] M. Mehl, B. Uekermann, H. Bijl, D. Blom, B. Gatzhammer, A. van Zuijlen, Parallel coupling numerics for partitioned fluid–structure interaction simulations, Comput. Math. Appl. 71 (4) (2016) 869–891, http://dx.doi.org/10.1016/j.camwa.2015.12.025.
[12] A. Jameson, S. Shankaran, An assessment of dual-time stepping, time spectral and artificial compressibility based numerical algorithms for unsteady flow with applications to flapping wings, in: 19th AIAA Computational Fluid Dynamics, 2009, http://dx.doi.org/10.2514/6.2009-4273.
[13] L. Martinelli, A. Jameson, F. Grasso, A multigrid method for the Navier Stokes equations, in: 24th Aerospace Sciences Meeting, 1986, http://dx.doi.org/10.2514/6.1986-208.
[14] M. Morelli, T. Bellosta, A. Guardone, Efficient radial basis function mesh deformation methods for aircraft icing, J. Comput. Appl. Math. (2021) 113492, http://dx.doi.org/10.1016/j.cam.2021.113492.
[15] L. Abergo, M. Morelli, A. Guardone, Aerodynamic shape optimization based on discrete adjoint and RBF, J. Comput. Phys. (2023) 111951, http://dx.doi.org/10.1016/j.jcp.2023.111951.
[16] P. Masarati, M. Morandini, P. Mantegazza, An efficient formulation for general-purpose multibody/multiphysics analysis, 2014, http://dx.doi.org/10.1115/1.4025628.
[17] O.A. Bauchau, P. Betsch, A. Cardona, J. Gerstmayr, B. Jonker, P. Masarati, V. Sonneville, Validation of flexible multibody dynamics beam formulations using benchmark problems, Multibody Syst. Dyn. 37 (2016) 29–48.
[18] A. Cocco, A. Savino, D. Montagnani, M. Tugnoli, F. Guerroni, M. Palazzi, A. Zanoni, A. Zanotti, V. Muscarello, Simulation of tiltrotor maneuvers by a coupled multibody-mid fidelity aerodynamic solver, in: 46th European Rotorcraft Forum (ERF 2020), Russian Helicopters, 2020, pp. 106–112.
[19] Y. Liu, Q. Xiao, A. Incecik, A coupled CFD/Multibody dynamics analysis tool for offshore wind turbines with aeroelastic blades, in: International Conference on Offshore Mechanics and Arctic Engineering, Vol. 57786, American Society of Mechanical Engineers, 2017, http://dx.doi.org/10.1115/OMAE2017-61062, V010T09A038.
[20] G.L. Ghiringhelli, P. Masarati, P. Mantegazza, Multibody implementation of finite volume C beams, AIAA J. 38 (1) (2000) 131–138, http://dx.doi.org/10.2514/2.933.
[21] P. Masarati, M. Lanz, P. Mantegazza, Multistep integration of ordinary, stiff and differential-algebraic problems for multibody dinamics applications, in: Xvi Congresso Nazionale AIDAA, 2001, pp. 1–10.
[22] O.A. Bauchau, L. Trainelli, The vectorial parameterization of rotation, Nonlinear Dynam. 32 (1) (2003) 71–92, http://dx.doi.org/10.1023/A:1024265401576.

[23] J. Degroote, P. Bruggeman, R. Haelterman, J. Vierendeels, Stability of a coupling technique for partitioned solvers in FSI applications, Comput. Struct. 86 (23–24) (2008) 2224–2234, http://dx.doi.org/10.1016/j.compstruc.2008.05.005.
[24] S. Etienne, D. Pelletier, A general approach to sensitivity analysis of fluid–structure interactions, J. Fluids Struct. 21 (2) (2005) 169–186, http://dx.doi.org/10.1016/j.jfluidstructs.2005.07.001.
[25] A. Rusch, Extending SU2 to fluid-structure interaction via preCICE, (Bachelor's Thesis), Technische Universität München, 2016.
[26] E. Ramm, W. Wall, Fluid-structure interaction based upon a stabilized (ALE) finite element method, in: 4th World Congress on Computational Mechanics: New Trends and Applications, CIMNE, Barcelona, 1998, pp. 1–20.
[27] M.W. Scroggs, J.S. Dokken, C.N. Richardson, G.N. Wells, Construction of arbitrary order finite element degree-of-freedom maps on polygonal and polyhedral cell meshes, ACM Trans. Math. Softw. 48 (2) (2022) 1–23.
[28] H. Matthies, J. Steindorf, Partitioned strong coupling algorithms for fluid-structure interaction, Comput. Struct. 81 (2003) 805–812, http://dx.doi.org/10.1016/S0045-7949(02)00409-1.
[29] W. Dettmer, D. Perić, A fully implicit computational strategy for strongly coupled fluid–solid interaction, Arch. Comput. Methods Eng. 14 (2007) 205–247, http://dx.doi.org/10.1007/s11831-007-9006-6.
[30] C. Wood, A. Gil, O. Hassan, J. Bonet, A partitioned coupling approach for dynamic fluid–structure interaction with applications to biological membranes, Internat. J. Numer. Methods Fluids 57 (2008) 555–581, http://dx.doi.org/10.1002/fld.1815.
[31] C. Kassiotis, A. Ibrahimbegovic, R. Niekamp, H. Matthies, Nonlinear fluid-structure interaction problem. Part I: Implicit partitioned algorithm, nonlinear stability proof and validation examples, Comput. Mech. 47 (2011) 305–323, http://dx.doi.org/10.1007/s00466-010-0545-6.
[32] H. C., R. S., B. D., H.J.-L.L. T., G. A., V. D., P. H., Partitioned solver for strongly coupled fluid-structure interaction, Comput. & Fluids 71 (11 - 12) (2013) 793–801, http://dx.doi.org/10.1016/j.compfluid.2012.11.004.
[33] B. Froehle, P.-O. Persson, A high-order discontinuous Galerkin method for fluid–structure interaction with efficient implicit–explicit time stepping, J. Comput. Phys. 272 (2014) 455–470, http://dx.doi.org/10.1016/j.jcp.2014.03.034.
[34] M. Morelli, T. Bellosta, A. Guardone, Development and preliminary assessment of the open-source CFD toolkit SU2 for rotorcraft flows, J. Comput. Appl. Math. 389 (2021) 113340, http://dx.doi.org/10.1016/j.cam.2020.113340.